Journal of Applied Electrochemistry **34**: 885–890, 2004.

Electrochemical insertion of lithium into graphite–zinc composites

A. DAILLY[1], J. GHANBAJA[1], P. WILLMANN[2] and D. BILLAUD[1,*]
[1]*Laboratoire de Chimie du Solide Minéral, UMR 7555, UHP-Nancy I, BP 239, 54506 Vandoeuvre-les-Nancy Cedex, France*
[2]*CNES, 18 Avenue E. Belin, 31055 Toulouse Cedex, France*
*(*author for correspondence, fax : +33-0-3-83-68-46-23, e-mail: denis.billaud@lcsm.uhp-nancy.fr)*

Received 11 February 2004; accepted in revised form 23 March 2004

Key words: graphite intercalation compound, lithium alloy composite electrodes, Li_xZn alloy, reduction

Abstract

Metal-based composites are currently under investigation as possible negative-electrode materials in lithium-ion batteries. We present here a new composite material composed of zinc particles deposited mainly onto graphite surfaces. This Zn/graphite composite was prepared by reduction of zinc chloride $ZnCl_2$ by a KC_8 graphite intercalation compound in tetrahydrofuran. Electrochemical insertion of lithium occurs both in graphite and in zinc. A stable specific charge of 355 mAh g^{-1} is obtained starting from the third charge/discharge cycle. As in Sb/graphite composites prepared by the same technique, the stabilizing role of graphite against metal fragmentation and pulverization is demonstrated.

1. Introduction

Present day commercial rechargeable lithium-ion battery negative electrodes are based on electro-active carbonaceous materials because they exhibit both a relatively high reversible capacity, at a potential close to that of metallic lithium, and a long cycle life. Nevertheless, since research and development activities are focused mainly on higher specific charges and energy densities, a renewed interest has developed in lithium alloy electrodes as alternatives to carbon-based intercalation materials. In addition to their low operating voltage vs lithium, these alloys exhibit large theoretical energy densities. The major drawback associated with lithium alloys as negative electrodes includes a large volume dilatation and contraction during alloying/dealloying of lithium into/from metallic matrices. This generates high mechanical stresses, which tend to decrepitate the host matrix after a few cycles. Ultimately, the capacity is reduced considerably due to the loss of electrical integrity between the particles produced by decrepitation and the current collector.

Many attempts to improve the dimensional stability of lithium alloys during cycling have been reported. The concept of supporting small particles of electro-active lithium alloys with a less active or non-active matrix was introduced in 1981 [1]. Numerous studies have been conducted on electrode materials involving graphite and fine metal particles [2–4]. Electrochemical alloying of lithium with zinc has shown that a number of stable crystalline phases can be produced [5]. The theoretical specific capacity of pure zinc is 412 mAh g^{-1}, greater than the theoretical capacity of 372 mAh g^{-1} for graphitic carbons. In this work, we report on the synthesis of Zn-based graphite compounds in which the graphite host provides not only a conductive matrix for the dispersed metal phase, but also acts as an electrochemically active material for lithium insertion and removal. This composite material was prepared by the reduction of $ZnCl_2$ by the stage-1 potassium graphite intercalated compound (GIC), KC_8, in a tetrahydrofuran (THF) medium. This process, described by Braga [6], leads to materials, the structure of which is still being debated. Some studies indicate that the reaction leads to intercalated metal into graphite whereas others suggest that the formation of supported metallic clusters on the graphite surface takes place [7, 8]. To address this controversy, we have performed our own synthesis and studied the reaction products by X-ray diffraction and transmission electron microscopy. Finally we investigated this anode material in a lithium-ion half-cell.

2. Experimental

The starting material KC_8 was prepared using the usual two-zone method [9]. The intercalation reaction was performed in the vapor phase with a temperature difference of 5 °C between the alkali metal ($T_K = 250$ °C) and the host sample (Ceylon graphite, average size granulometry: 25–45 μm) ($T = 255$ °C) [9]. KC_8 is known to be a strong reducing agent. Consequently, a dispersion of KC_8

in tetrahydrofuran is expected to provide a complex medium for the reduction of anhydrous $ZnCl_2$ when dissolved in tetrahydrofuran. The reaction was carried out at room temperature, under an argon atmosphere, by gradually adding the $ZnCl_2$/tetrahydrofuran solution into the KC_8/tetrahydrofuran dispersion. After 4 h the solution was filtered out and the product was repeatedly washed with anhydrous tetrahydrofuran and dried under vacuum.

Powder X-ray diffractometry using an automated powder diffractometer with Mo $K\alpha$ radiation (Rotaflex RU-200B, RIGAKU generator and CPS 120 INEL detector, transmission assembly) and transmission electron microscopy (Philips CM20 instrument operated at 200 kV) were used to examine the composite structure and morphology, respectively. The electrode was made from the as-synthesized composite in an argon glove bag. A 1-methyl-2-pyrrolidon slurry of 90 wt% of Zn-based graphite anode material, added to 10 wt% of polyvinylidene fluoride (PVDF) binder were used to coat a thick copper current collector. This coated collector was assembled into a test cell using a Li counter electrode acting also as a reference electrode. The electrolyte was composed of $LiClO_4$ (1 M) in ethylene carbonate (EC). The electrochemical tests were performed using a Mac Pile II, potentiostat-galvanostat (Biologic) working both in the cyclic voltammetric mode between 0 and 2 V vs Li/Li^+ with following steps of 2.5 mV every 2 min and in the galvanostatic mode. A constant current density for charge (reduction) and discharge (oxidation) of 7 μA mg^{-1} between 0 and 2 V vs Li^+/Li was applied for 6 min and the circuit was then opened for 10 s as a relaxation condition.

3. Results and discussion

The X-ray diffraction pattern resulting from the reaction of $ZnCl_2$ with KC_8 in tetrahydrofuran medium, displayed in Figure 1, clearly shows four phases, identified as graphite, potassium chloride, zinc metal and zinc oxide. Potassium atoms previously intercalated in the pristine KC_8 appear to be largely deintercalated as evidenced by the formation of KCl, which precipitates in tetrahydrofuran because of its extremely low solubility in this solvent and the strong 0 0 2 reflection at 336 pm due to the recovered graphite. The broadening of this last reflection indicates that the deintercalation and further reduction generate a degree of disorder, as shown by the coherence length (size of the coherent domains) along the c-direction of graphite, L_C. L_C was approximated by analysis of the full width at half height of the 0 0 2 reflection using the Scherrer equation ($L_C = 0.9\lambda/\beta\cos\theta$), and determined to be ≈29 nm. Two reflections corresponding to the original $ZnCl_2$ material are still present because of its introduction in excess in the reaction medium. The presence of zinc oxide may be explained by the fact that zinc metal can be oxidized easily and that synthesis conditions did not allow for the complete removal of oxygen and moisture. A direct analysis of the microstructure of the sample was performed by TEM. The EDX spectrum and the associated selected area electron diffraction (SAED) pattern of free metal clusters are displayed in Figure 2a and 2b, respectively. The intense, discontinuous and finely polycrystalline rings pattern of the electron diffraction pattern indicate that these clusters are composed mainly of potassium chloride and zinc metal. The EDX spectrum identifies the presence of K, Cl, and Zn and some O. The images clearly illustrate the

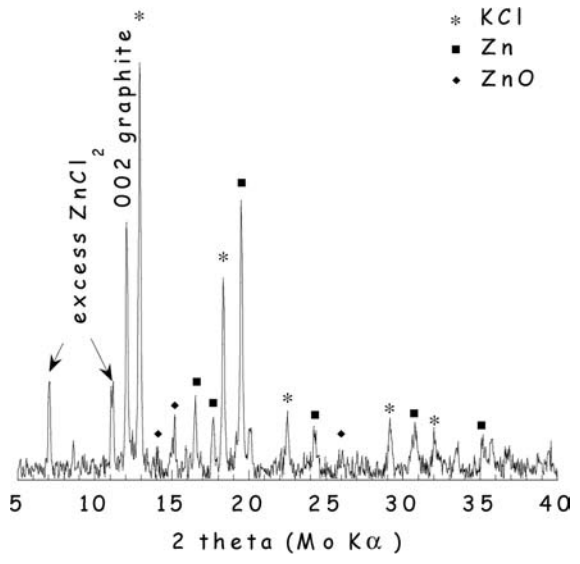

Fig. 1. X-ray diffraction pattern of zinc-based graphite compound prepared by reduction of $ZnCl_2$ with KC_8 in tetrahydrofuran.

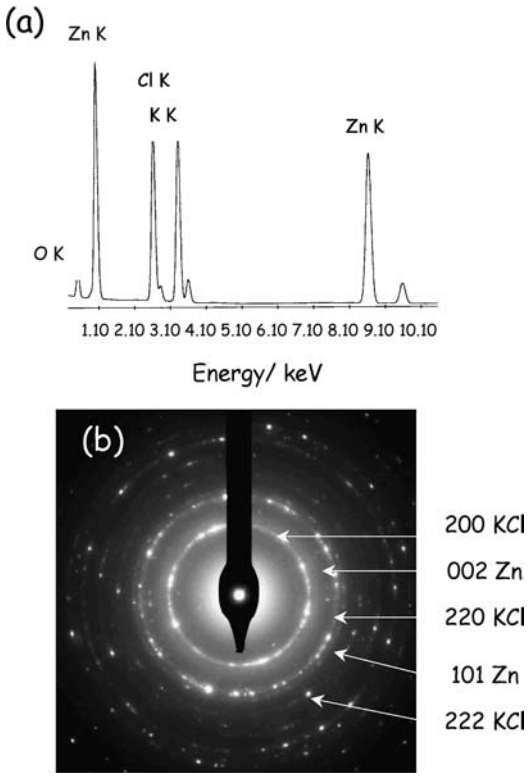

Fig. 2. (a) EDX spectrum and (b) SAED pattern of free clusters.

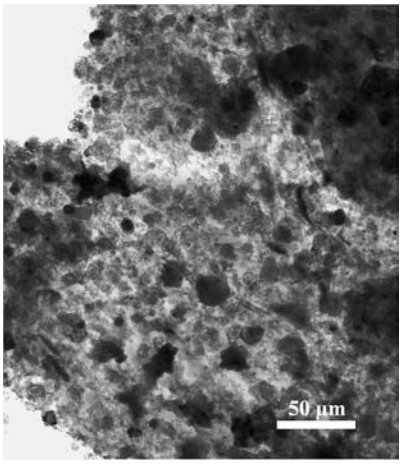

Fig. 3. Bright-field micrograph of the graphite surface obtained after $ZnCl_2$ reduction by KC_8.

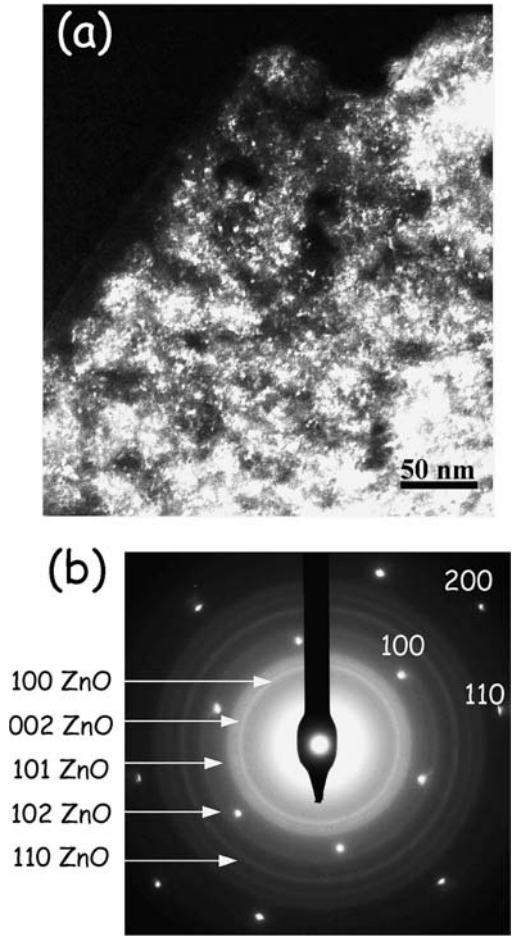

Fig. 4. (a) Dark-field micrograph and (b) SAED pattern of ZnO supported graphite.

heterogeneity of the material with the presence of crystalline and amorphous regions. The bright-field micrograph of the graphite surface (Figure 3) gives evidence for the coexistence of potassium chloride and zinc particles. Their sizes are larger than nano-scale and crystalline particles supported on graphite shown on the dark-field micrograph displayed in Figure 4a. The SAED pattern of the graphite surface (Figure 4b) shows the expected graphite hk0 spots superimposed on the intense and narrow rings that are indexed as zinc oxide (ZnO). It is likely that zinc metal exhibits an amorphous character and that only zinc oxide particles diffract. It should be noted that graphitic regions showing such characteristics are a minority. TEM analysis corroborates X-ray diffraction measurements and also indicates that zinc is not intercalated between graphite layers to form a graphite intercalation or included (without charge transfer) compound, contrary to the conclusion of Braga [6]. The synthesized product obtained after reduction of $ZnCl_2$ by KC_8 has a heterogeneous nature. Various phases coexist. Zinc is present outside the graphite layers and associated with potassium chloride in the shape of free three-dimensional clusters or small nodules supported on the graphite surface and nano-sized oxide particles deposited on the graphite.

The behavior of the Zn-based graphite composite used as negative electrode material in lithium-half cell is shown in the cyclic voltammograms curves in Figure 5. They exhibit electrochemical activity of both graphite and zinc when referenced to voltammograms obtained for graphite alone. A broad peak centered on 0.5 V was evidenced during the first reduction. Compared to pure graphite, this irreversible reaction is more pronounced in the case of the Zn-based graphite composite. This peak can be attributed in part to the formation of the solid-electrolyte interphase (SEI) on both graphite and metal [10]. The electrolyte reduction products are expected to form throughout a reaction of the lithium with the solvent and the salt. EC is well known to be a good filming agent. Usually the metal anode/passivating layer varies during cycling due to the large volume changes. Thus filming reactions may extend over a large number of cycles. New SEI is likely to be formed on fresh and exposed surface of the active material. In a recent report, the discharge curve of a cell with a ZnO electrode cycling against lithium, was shown to exhibit a large plateau at 0.6 V followed with a well-defined one at 0.2V [11, 12]. These results are consistent with those generally described for the tin oxides. This irreversible reaction occurs mainly in the first cycle. Due to our preparation method, the sample contains oxide impurities, which might be irreversibly reduced during the first lithium uptake. The alloying of the remaining lithium with elemental metal follows it. In subsequent cycles the lithium is reversibly alloyed with the metal while the Li_2O remains inactive [13]. This first phenomenon contributes to a great extent, to the irreversible capacity loss of the anode. In the second and the subsequent cycles, peaks are still observable to voltage levels that match with those reported by Belliard et al. [14] for the galvanostatic test of ZnO, and the earlier work done by Fujieda et al. [15] on a zinc electrodeposited electrode. The formation of the different Li_xZn phases is evidenced on the voltammograms during the oxidation process. Peaks related to three lithium–zinc alloys appear at 0.24, 0.5 and 0.64 V corresponding to the formation of

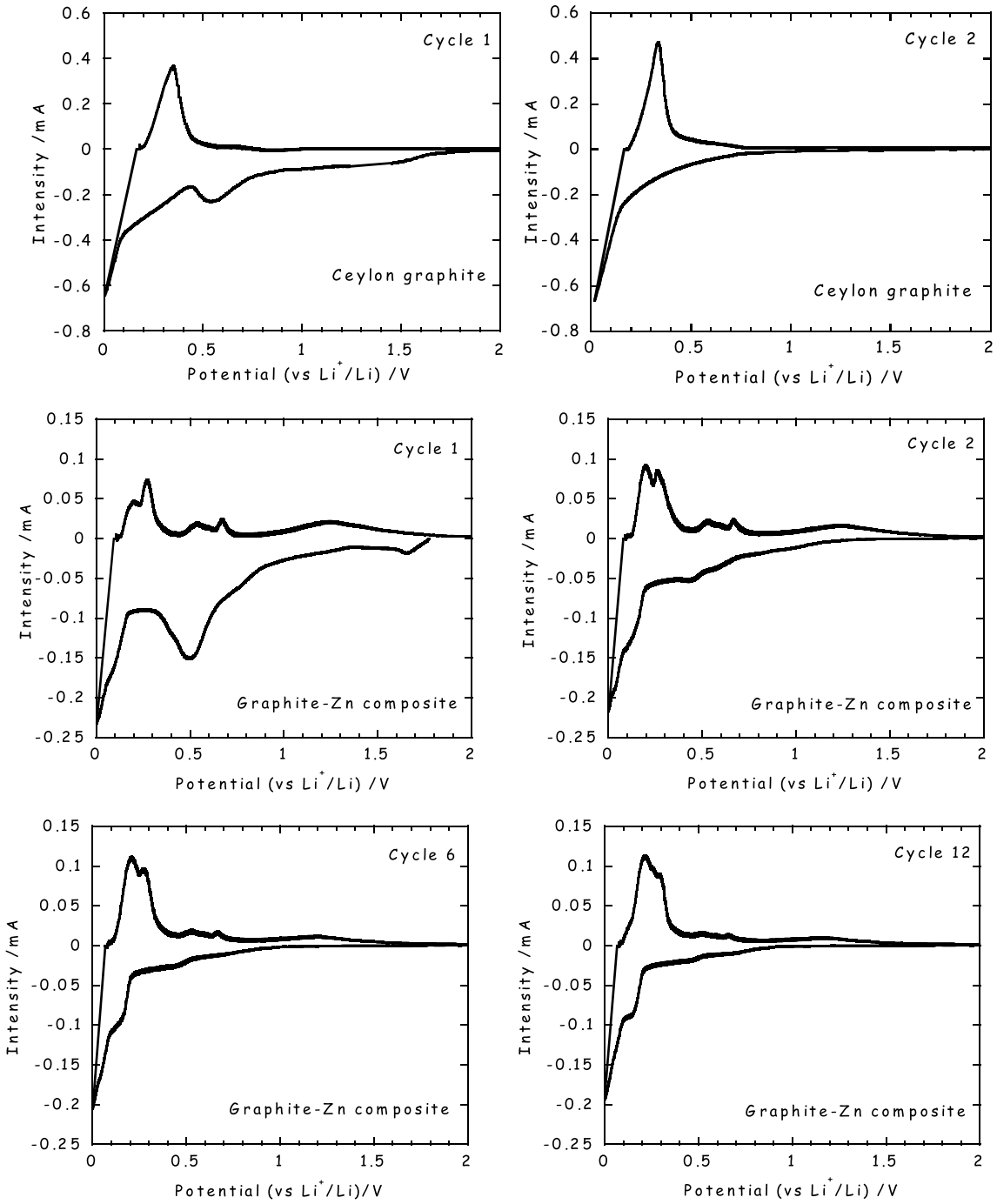

Fig. 5. Cyclic voltammograms of zinc-based graphite composite as negative electrode material.

Li_2Zn_3, $LiZn_2$ and Li_2Zn_5 respectively, whereas the peak associated with LiZn (0.18 V) might be convolved with the peak associated with lithium intercalation and deintercalation into graphite. We believe that peaks related to both contributions of graphite and metal are superimposed at low potentials. The graphite seems to recover good reversibility during the cycling if we consider the progressive increase of the oxidation peak. It is likely that the little disorder of the host graphite structure that occurs with potassium deintercalation and with further $ZnCl_2$ reduction interrupts the reversible lithium insertion between graphite layers. Another phenomenon in the voltammogram during the oxidation process between 0.75 and 1.6 V is observed. It was reported previously [14] but is still unexplained even if considered as a zinc contribution. Observing the evolution of the voltammograms upon cycling shows that even though there is a progressive loss of the capacity attributed to the zinc there still remains a contribution. While cyclic voltammetry is an effective way to observe the various phenomena occurring during the cycling, galvanostatic measurements are more appropriate for estimating the capacity of the material. Figure 6 shows charge/discharge curves of the Zn-based graphite

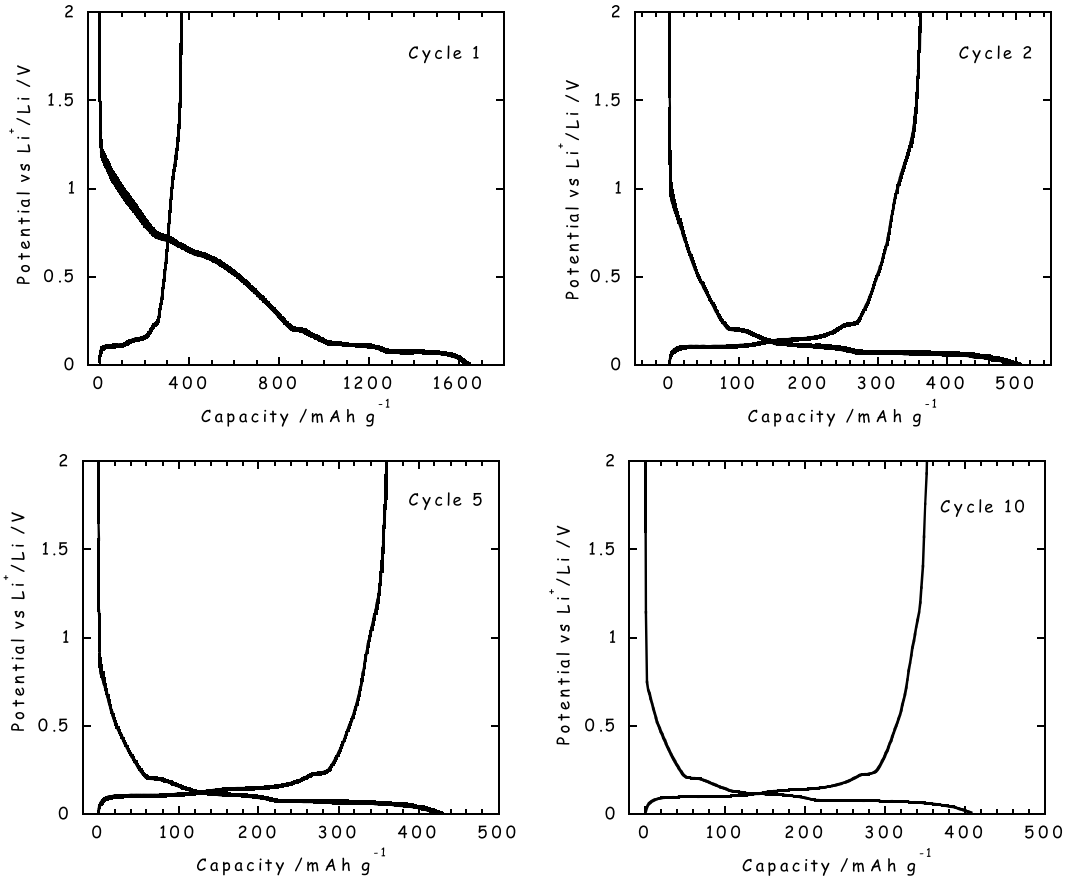

Fig. 6. Galvanostatic curves of zinc-based graphite compound obtained after $ZnCl_2$ reduction by KC_8.

composite investigated as a negative electrode. In the first reduction process, long potential multi plateaus and a large capacity loss may be attributed to the irreversible reactions, like the formation of the passivation film and the zinc oxide conversion into metal. In addition to these irreversible processes, the formation of the lithiated phases Li_xZn and the lithium graphite intercalation stages occurs simultaneously. Small shoulders for potentials near 0.5 and 1 V are in evidence on the oxidation curve. These correspond respectively, for the first one, to the deinsertion of the Li_2Zn_5 and $LiZn_2$ phases, and for the second, to the supplementary phenomenon already observed on voltammograms between 0.75 and 1.6 V associated to a hypothesized behavior particular to zinc oxide. The total reversible capacity of the graphite-zinc system between 0 and 2 V is close to 380 mAh g^{-1} for the first cycle, and reaches a value of 355 mAh g^{-1} to the tenth cycle. Such a value is still higher than that expected by considering only the amount of graphite present in the electrode (277 mAh g^{-1}). The capacity of Zn decays from 104 mAh g^{-1} to about 78 mAh g^{-1} at the third cycle, assuming the constancy of the reversible graphite capacity. The irreversible capacity remains high upon cycling as observed in the voltammograms. Volumetric changes in alloy phases are considered to be responsible for the capacity loss. Parts of the passivating layer that cannot withstand the volume expansion of Li_xZn alloy during cycling may break up, allowing fresh surface of active material to be exposed to the electrolyte, resulting in the formation of a new solid interphase and a concomitant consumption of charge. The evolution of the cycle capacity is highlighted in Figure 7. This capacity reaches a stable value quickly, contrary to what is observed for the $ZnO:SnO_2$ (1:1) precursor studied by Belliard et al. [14] in which the reversible capacity shows a regular decrease during cycling. In our Zn/graphite composites only about 25 wt% Zn is inactive at the first charge/discharge cycle. The steady reversible capacity is close to that expected for pristine Ceylon graphite. Therefore, our composites do not

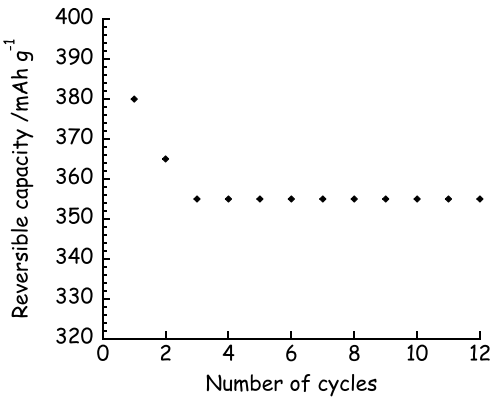

Fig. 7. Reversible capacity evolution during the cycling.

improve electrochemical performance in comparison to graphite. However, the stabilizing role of graphite against metal pulverization is observed in the Zn/graphite system as has been noted for Sb/graphite composites [16].

4. Conclusion

The reduction of $ZnCl_2$ by KC_8 in tetrahydrofuran medium leads to the formation of products associating deintercalated graphite and zinc particles. The composite microstructure was found to be complex with the presence of crystalline and amorphous regions. These products have been tested as active materials for the insertion of lithium. Cyclic voltammograms and galvanostatic curves display two series of reactions appearing both in reduction and oxidation processes. One is related to lithium intercalation into graphite, while the other is associated with the lithium alloying of zinc. Evidence for irreversible capacity upon prolonged cycling indicates that while graphite can usually play the role of stabilizing matrix, is not enough efficient in this case in containing the volume changes that occur during the Li_xZn alloying/dealloying. However, the presence of graphite allows a large part of Zn to be cycled reversibly. The reversible capacity of the composite is close to 355 mAh g^{-1}, a value comparable to that of pristine Ceylon graphite. Therefore, the Zn/graphite composites obtained by reduction of $ZnCl_2$ by KC_8 do not improve electrochemical performances in comparison to graphite. However, the presence of graphite prevents the metal from particle pulverization that generally occurs during lithium alloying as previously observed with Sb/composites [16].

References

1. B.A. Boukamp, G.C. Lesh and R.A. Huggins, *J. Electrochem. Soc.* **128** (1981) 725.
2. G.X. Wang, J.H. Ahn, M.J. Lindsay, L. Sun, D.H. Bradhurst, S.X. Dou and H.K. Liu, *J. Power Sources* **97–98** (2001) 211.
3. J.Y. Lee, R. Zhang and Z. Liu, *J. Power Sources* **90** (2000) 70.
4. J. Yang, Y. Takeda, N. Imanishi, T. Ichikawa and O. Yamamoto, *J. Power Sources* **79** (1999) 220.
5. J. Wang, P. King and R.A. Huggins, *Solid State Ionics* **20** (1986) 185.
6. D. Braga, A. Ripamonti, D. Savoia, C. Trombini and A. Umani-Ronchi, *J. Chem. Soc.* (1978) 927.
7. A. Messaoudi, R. Erre and F. Béguin, *Carbon* **29** (1991) 4/5 515.
8. M. Inagaki, Y. Shiwachi and Y. Maeda, *J. de Chimie Physique* **81** (1984) 11/12 847.
9. A. Hérold, *Bul. Soc. Chim.* (1955) 999.
10. M. Wachtler, J.O. Besenhard and M. Winter, *J. Power Sources* **94**, (2001) 189.
11. F. Belliard, P.A. Connor and J.T.S. Irvine, *Solid State Ionics* **135** (2000) 163.
12. H. Li, X. Huang and L. Chen, *Solid State Ionics* **123** (1999) 189.
13. R.A. Huggins, *Solid State Ionics* **115** (1998) 57.
14. F. Belliard and J.T.S. Irvine, *J. Power Sources* **97–98** (2001) 219.
15. T. Fujieda, S. Takahashi and S. Higuchi, *J. Power Sources* **40** (1992) 283.
16. A. Dailly, J. Ghanbaja, P. Willmann and D. Billaud, *Electrochim. Acta* **48** (2003) 977.